Available online at www.sciencedirect.com
ScienceDirect
Trans. Nonferrous Met. Soc. China 21(2011) 15−25
Transactions of Nonferrous Metals Society of China
www.tnmsc.cn

Microstructure evolution and mechanical properties of Mg-*x*%Zn-1%Mn (*x*=4, 5, 6, 7, 8, 9) wrought magnesium alloys

ZHANG Ding-fei[1, 2], SHI Guo-liang[1], ZHAO Xia-bing[1], QI Fu-gang[1]

1. College of Materials Science and Engineering, Chongqing University, Chongqing 400045, China;
2. National Research Center for Magnesium Alloys, Chongqing 400044, China

Received 22 October 2009; accepted 19 October 2010

Abstract: The roles of Zn content and thermo-mechanical treatment in affecting microstructures and mechanical properties of Mg-*x*%Zn-1%Mn (mass fraction, *x*=4, 5, 6, 7, 8, 9) wrought Mg alloys were investigated. The microstructure was extremely refined by dynamic recrystallization (DRC) during extrusion. With increasing Zn content, the DRC grains tended to grow up, at the same time, more second phase streamlines would be present, which restricted the further growing. During solution treatment, the DRC grains would rapidly grow up; however, higher Zn content could hinder the grain boundary expanding, which results in finer ultimate grains. $MgZn_2$ dispersoid particles which are coherent with the matrix would precipitate from the supersaturated solid solution during the one-step aging process, and nano-sized GP zones formed during the pre-aging stage of the two-step aging provide a huge amount of effective nuclei for the $MgZn_2$ phases formed in the second stage, which makes the $MgZn_2$ particles much finer and more dispersed. The mechanical properties of as-extruded samples were not so sensitive to the variation of Zn content, the tensile strength fluctuates between 300 and 320 MPa, and the elongation maintains a high value between 11% and 14%. The strength of aged samples rises as a parabolic curve with increasing Zn content, specifically, the tensile strength of one-step aged samples rises from 278 to 374 MPa, and that of two-step aged ones rises from 284 to 378 MPa, yet the elongation of all aged samples is below 8%. When Zn content exceeds its solid solution limit in Mg-Zn system (6.2%, mass fraction), the strength rises slowly but the elongation deteriorates sharply, so a Mg-Zn-Mn alloy with 6% Zn possesses the best mechanical properties, that is, the tensile strengths after one- and two-step aging are 352 and 366 MPa, respectively, and the corresponding elongations are 7.98% and 5.2%, respectively.
Key words: Mg-Zn-Mn alloy; two-step aging; age-hardening; Zn content

1 Introduction

Considerable attention has been focused on a series of newly designed Mg-Zn-Mn (ZM) wrought magnesium alloys, since high strength can be achieved after thermal deformations such as extrusion, forging and rolling, or after particular heat treatments such as solution treatment and ageing. On the other hand, alloys of this series contain no noble metal elements such as Zr, so lower cost can simply make them more widespread.

Mg-Zn alloys are the most widely used wrought magnesium alloys which form the basis of Mg-Zn-Mn series alloys. Since the Mg-Zn alloy system is age-hardenable, there is a great potential to improve the strength by various heat treatments and micro-alloying. It is generally accepted that, for Mg-Zn alloys containing 4%−9% Zn and aged isothermally at 120−260 °C, the strengthening precipitate phases are β_1' and β_2'. The metastable phase β_1', also described as MgZn′, forms as rods with its long axis parallel to the $[0001]_\alpha$ direction of the α-Mg matrix, while the metastable phase β_2' forms as plates on $(0001)_\alpha$. Historically, it is determined that both β_1' and β_2' phases have a hexagonal structure (a=0.520 nm, c=0.857 nm) that is identical to that of the Laves phase $MgZn_2$. In a newly published paper, it was found that the β_1' phase mainly formed as $[0001]_\alpha$ rods, unlike the $MgZn_2$ structure, a base-centered monoclinic structure is formed (a=2.596 nm, b=1.428 nm, c=0.524 nm, γ=102.5°) similar to that of the Mg_4Zn_7 phase[1−7]. In the development of the equilibrium β phase during the precipitation heat treatment, several transition phases are formed in a specific sequence: supersaturated solid solution(SSSS)→solute clusters→GP zones→β_1' (rods

Foundation item: Project(2007CB613700) supported by the National Basic Research Program of China; Project(2007BAG06B04) supported by the National Science and Technology Pillar Program During the 11th Five-Year Plan Period, China; Project(50725413) supported by the National Natural Science Foundation of China; Project(CDJXS10132202) supported by the Fundamental Research Funds for the Central Universities, China
Corresponding author: SHI Guo-liang; Tel: +86-13193083536; E-mail: sglholo@yahoo.com.cn
DOI: 10.1016/S1003-6326(11)60672-9

and blocky precipitates $\perp\{0001\}_{Mg}$; $MgZn_2$ or possible $Mg_4Zn_7 \rightarrow \beta_2'$ (coarse plates $//\{0001\}_{Mg}$ and laths $\perp[0001]_{Mg}$; $MgZn_2) \rightarrow \beta$ equilibrium phase (MgZn or Mg_2Zn_3)[8]. The decomposition of the SSSS initially occurs through clustering of solute atoms. Depending on the ageing temperature (mainly below 100 °C) and alloy composition, three types of coherent GP zones may form: GP1 zones as plates on $\{11\bar{2}0\}_{Mg}$, GP2 zones as oblate spheroids on $\{0001\}_{Mg}$ and GP3 zones as discs on $\{0001\}_{Mg}$[6−11]. Recently, spherical GP zones containing a high concentration of Zn were discovered in the ZM61 sample aged at 70 °C for 48 h using TEM and atom probe. GP zones can act as heterogeneous nucleation sites for the transition phases β_1' and β_2' during high temperature aging, resulting in finer microstructure as well as enhanced age hardening response, that is why two-step aging has a better strengthening effect than traditional artificial aging[9−12].

Magnesium and its alloys with a HCP crystal structure have few active slip systems, so their deformability is quite poor. Among the currently employed large-scale manufacturing processes, extrusion is the best method for breaking a cast structure, because the billet is subjected to compressive stresses only, the hot extrusion is commonly used to produce wrought magnesium alloy products such as long bars or tubes in complex cross-sectional shapes. The major disadvantage of extrusion process is that whether an inhomogeneous metal flow may appear and consequently undesirable mechanical and metallurgical features including surface cracking and recrystallization could be eliminated depending on the shape of the alloy[13−14]. In a previous study, Mg-6%Zn-1%Mn (ZM61) alloy could be smoothly extruded at 310 °C with completely dynamic recrystallization during the hot-extrusion, its strength after two-step aging could reach that of a commercial wrought magnesium alloy ZK60[15].

The present work reports the microstructures and tensile properties of Mg-*x*%Zn-1%Mn alloys with varying mass fraction of Zn (*x*=4, 5, 6, 7, 8, 9) after extrusion and two kinds of aging treatments.

2 Experimental

Cast ingots with nominal compositions of Mg-*x*%Zn-1%Mn (*x*=4, 5, 6, 7, 8, 9, mass fraction, the same below) were prepared by the direct chill semi-continuous casting using high purity Mg(99.99%), Zn(99.99%) and Mg-4%Mn intermediate alloy (mass fraction). Hereafter, they are designated as ZM41, ZM51, ZM61, ZM71, ZM81 and ZM91 following commercial nomenclature, respectively. The chemical compositions of these alloys were analyzed by X-ray fluorescence spectrometer, and the results are listed in Table 1.

Six rods with size of *d* 80 mm×(220−250) mm were machined from these cast ingots. After being homogenized at 330 °C for 24 h, they were immediately inserted into the extrusion chamber and extruded at 350 °C with an extrusion ratio of 25. The detailed extrusion parameters are listed in Table 2.

Table 1 Chemical compositions of Mg-*x*%Zn-1%Mn alloys (mass fraction, %)

Alloy	Mg	Zn	Mn	Other
ZM41	95.02	4.00	0.95	0.02
ZM51	94.30	4.75	0.93	0.01
ZM61	93.27	5.77	0.94	0.02
ZM71	92.44	6.61	0.93	0.02
ZM81	91.14	7.86	0.96	0.04
ZM91	90.17	8.82	0.97	0.05

Table 2 Extrusion parameters of Mg-*x*%Zn-1%Mn wrought Mg alloys

Billet temperature/ °C	Mould temperature/ °C	Extrusion chamber temperature/ °C	Extrusion speed/ ($m \cdot min^{-1}$)	Extrusion ratio
330	350	390	0.2−2.8	25

Specimens for tensile test and microstructure analysis were cut from the extruded bars. They were solution treated at 420 °C for 2 h followed by water quenching (T4). The solution treated specimens were artificially aged at 180 °C for 16 h (T6). A two-step aging was carried out by pre-aging at 90 °C for 24 h, followed by aging at 180 °C for 16 h (T4+2-step aging). Water quenching was used after each aging step.

A dog-bone specimen with *d* 5 mm×50 mm was prepared for tensile test. Mechanical properties were tested on a Sans CMT−5105 electronic universal testing machine with a strain rate of 3 mm/min. The microstructure was analyzed by optical microscope and scanning electronic microscope (TESCAN VEGA Ⅱ LMU) equipped with the Oxford Inca energy dispersive spectrometer. As-cast specimens were etched with a dilute solution of 4% nitric acid in alcohol, and specimens in other states with a solution of picric acid and glacial acetic acid in alcohol. Phase analysis was conducted by a D/MAX−2500PC X-ray diffraction instrument using Cu K_α at a scanning rate of 4 (°)/min.

3 Results and discussion

3.1 Effect of Zn content on microstructures of as-cast and homogenized alloys

Fig.1 shows the micro structure of as-cast alloys. Dendritic crystals and interdendritic second-phases are

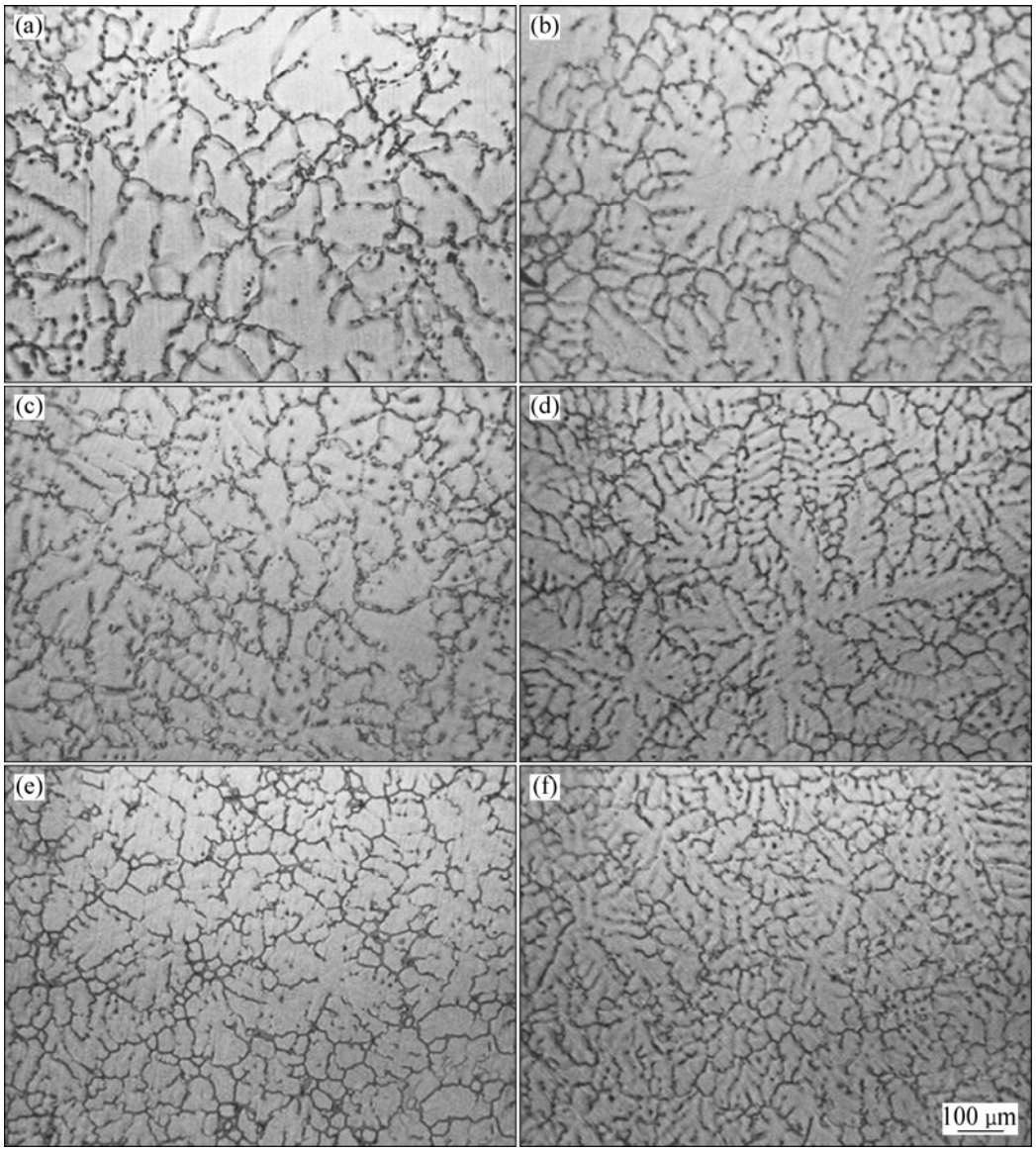

Fig.1 OM images of as-cast Mg-*x*%Zn-1%Mn alloys with different *x* values: (a) *x*=4; (b) *x*=5; (c) *x*=6; (d) *x*=7; (e) *x*=8; (f) *x*=9

present. High Zn content can refine dendritic crystals and increase interdendritic compounds, making the microstructure exhibit cellular structure in character.

Optical microscopy images of alloys in homogenized condition (Fig.2) show that those interdendritic Mg-Zn compounds partly redissolve into the α-Mg matrix resulting in light gray diffusion zones along both sides of the Mg-Zn networks or around Mg-Zn particles, which can soften alloys and benefit extrusion to some extent. As Zn content increases, those diffusion zones become wider.

The SEM micrograph and EDS results in Fig.3(a) and Table 3 present the typical microstructure of as-cast ZM91 alloy which is composed of dendritic α-Mg matrix, interdendritic Mg-Zn compounds and pure Mn particles, and this non-equilibrium microstructure is caused by fast cooling in the direct chill semi-continuous casting. Furthermore, low-melting alloy element such as Zn is mainly segregated to the interdendritic areas as the network structure, yet high-melting alloy element such as Mn mainly solves in the matrix, suggesting the characters of the dendritic segregation.

Diffusion zones are actually made up of thousands of much finer Mg-Zn particles (Fig.3(b)) which are precipitated in the course of Zn diffusing, corresponding

Table 3 EDS results of as-cast ZM91 alloy in Fig.3(a) (mass fraction, %)

Position	Mg	Mn	Zn	Total
A	42.94	0.68	56.38	100.00
B	52.24	0	47.76	100.00
C	50.68	0	49.32	100.00
D	95.79	1.12	3.51	100.00
E	45.39	0.70	53.91	100.00

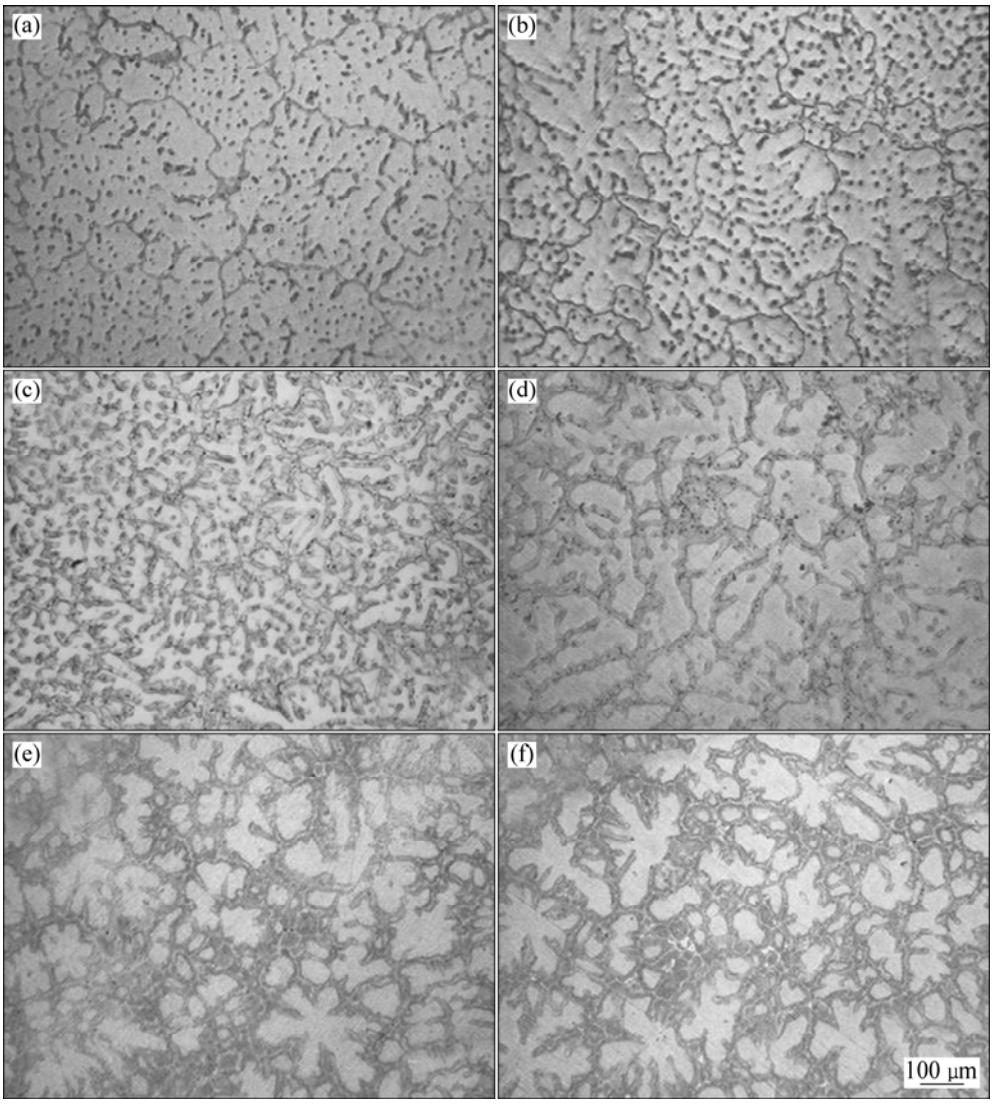

Fig.2 OM images of as-homogenized Mg-*x*%Zn-1%Mn Mg alloys with different *x* values: (a) *x*=4; (b) *x*=5; (c) *x*=6; (d) *x*=7; (e) *x*=8; (f) *x*=9

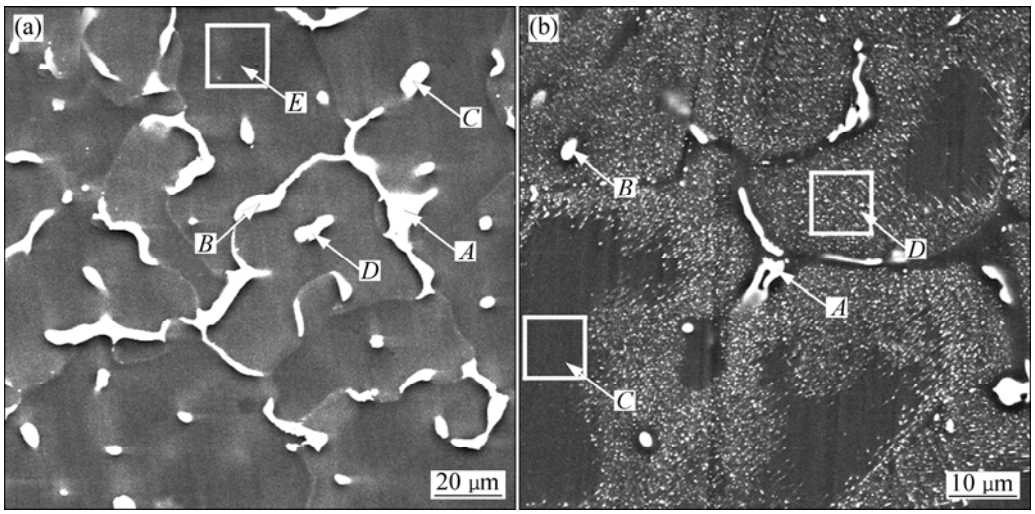

Fig.3 SEM images of as-cast (a) and as-homogenized (b) ZM91 alloys

EDS results are listed in Table 4. Precipitate-free zone (PFZ) is present in regions around those residual interdendritic Mg-Zn compounds. Fig. 4 shows the XRD pattern of as-homogenized ZM91 alloy. Apart from the well-defined Mg reflections, some additional peaks are detected, which are close to the reflections of $MgZn_2$, Mg_7Zn_3 and pure Mn. Particularly, the peak positions of $MgZn_2$ coincide well with those standard XRD patterns, suggesting that the main second phase in the homogenized condition is $MgZn_2$, and additional phases are Mg_7Zn_3 and pure Mn.

Table 4 EDS analysis results of as-homogenized ZM91 alloy in Fig.3(b) (mass fraction, %)

Position	Mg	Mn	Zn	Total
A	66.88	3.74	29.38	100.00
B	43.37	6.67	49.96	100.00
C	92.99	1.07	5.94	100.00
D	88.65	0.72	10.63	100.00

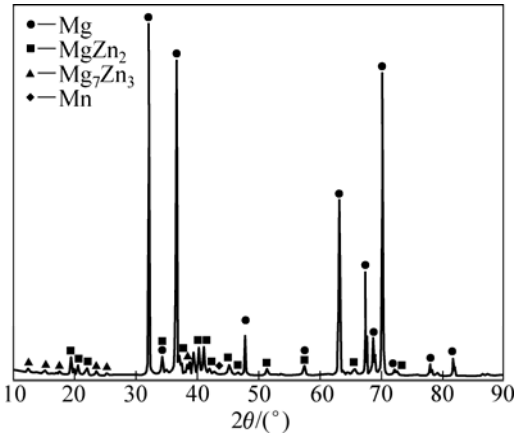

Fig.4 XRD pattern of as-homogenized ZM91 alloy

3.2 Effect of Zn content on microstructures of as-extruded alloys

Fig.5 shows the microstructures of as-extruded alloys, indicating that dynamic recrystallization (DRC)

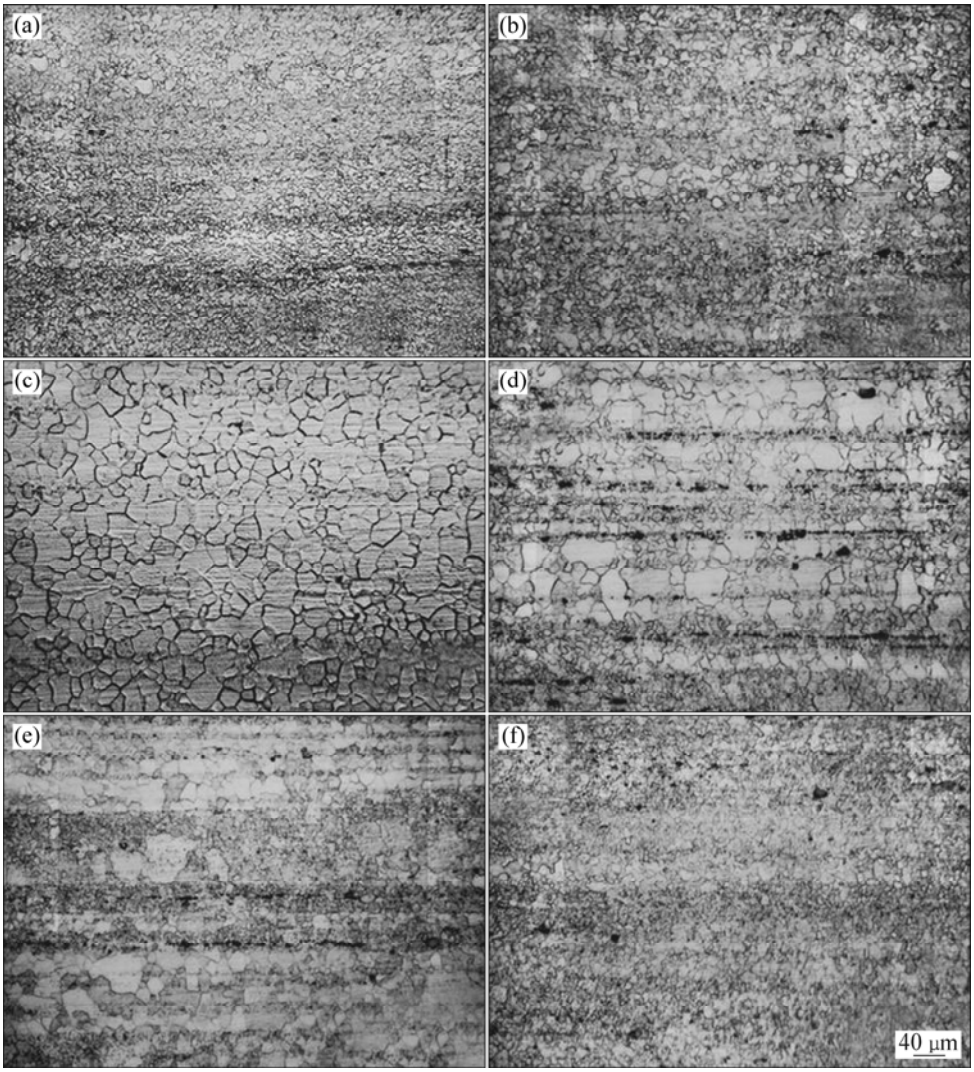

Fig.5 OM images of as-extruded Mg-*x*%Zn-1%Mn wrought Mg alloys with different *x* values: (a) *x*=4; (b) *x*=5; (c) *x*=6; (d) *x*=7; (e) *x*=8; (f) *x*=9 (parallel to extrusion direction)

occurs during the course of hot-extrusion. Visible second phase streamlines parallel to the extrusion direction lead to the increase of Zn content higher than 6% (mass fraction), which results in more intensive streamlines and consequently more non-uniform microstructure is obtained, that is grains in streamline areas are very thin but easy to abnormally grow up in the areas where microstructure is relatively clean. Streamlines initiated as particles in as-homogenized alloys are broken and routed to the extrusion direction at the push of a three-dimensional compressive stress field. These particles can act as effective nucleation sites for the DRC grains and also hinder their growth, so grains in streamline positions are much thinner. On the other hand, the DRC tends to be complete as the Zn content rises from 4% to 6%; elongated grains still can be seen in ZM41 alloy, yet most of the DRC grains grow up homogeneously in ZM61 alloy.

Figs.6(a)−(c) show the SEM micrographs of as-extruded ZM41, ZM61 and ZM91 alloys, respectively. All these alloys contain streamlines in their microstructures, yet streamlines in ZM41 alloy are much milder than those in ZM61 and ZM91alloys. On the other hand, the average DRC grain size of ZM41 alloy is less than 5 μm, but elongated strip grains that are not completely recrystallized are still present; the average grain size of ZM61 is about 15 μm and the streamlines start increasing. Streamlines in ZM91 alloy occupy nearly the entire microstructure.

After hot extrusion, ZM91 alloy reveals dense streamlines which comprise a great number of second phase particles, as shown in Fig.7. Fig.7 and Table 5 show the EDS analysis results, larger particles may originate from those residual interdendritic Mg-Zn compounds and pure Mn particles, while smaller ones may originate from thin Mg-Zn particles in diffusion zones of as-homogenized alloy.

Table 5 EDS results of as-extruded ZM91 alloy in Fig.7(b) (mass fraction, %)

Position	Mg	Si	Mn	Fe	Zn	Total
A	30.68	1.14	17.04	1.08	50.06	100.00
B	50.31	0	6.27	0	43.43	100.00
C	88.04	0	0.95	0	11.00	100.00

3.3 Effect of Zn content on microstructures of one-step and two-step aged alloys

Since the optical microstructures of one-step aged specimens are very similar to those of two-step aged ones, Fig.8 shows the microstructures of two-step-aged alloy (perpendicular to the extrusion direction), which were also observed by polarized light. DRC grains in different alloys have all grown up in the solution treatment. High Zn content puts a drag on grain growth,

Fig.6 SEM images of as-extruded Mg-*x*%Zn-1%Mn alloys with different *x* values: (a) *x*=4; (b) *x*=6; (c) *x*=9 (parallel to extrusion direction)

resulting in smaller final grain size. The grain size reduces remarkably as Zn content rises from 4% to 6%, but the reduction is not obvious when the Zn content is more than 6%.

Two-step aging adds one more aging process at temperature below 100 °C before the normal aging，the effect of this pre-aging on the microstructure is invisible

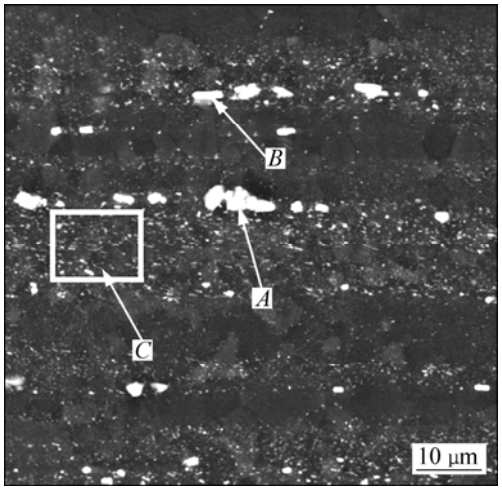

Fig.7 SEM microstructure of as-extruded ZM91 alloy

through optical microscope. Nano-sized GP zones formed during pre-aging process as well as metastable precipitates formed in the second-step aging can be clearly observed by transmission electron microscope (TEM). So optical micrographs only indicate the changes in both two- and one-step aged alloys.

SEM micrographs of ZM41, ZM61 and ZM91 alloys in T6 condition are shown in Fig.9. Contrast to as-extruded alloys (Fig.6), DRC grains after solution treatment and one-step aging distinctly grow up, especially in ZM41 alloy. Higher Zn content aggravates the lattice distortion and increases the residual second phase particles during solution treatment, so the resistance of grain growth is enhanced and thus smaller grains are formed at the end. In addition, most streamlines dissolve into matrix, but residual streamlines still can be seen in ZM91 alloy. The maximum solid solubility of Zn in the Mg-Zn system is 6.2% at the eutectic temperature 341 °C, so almost all Mg-Zn compounds in alloys with Zn content less than 6.2% (ZM41, ZM51 and ZM61) can dissolve into matrix at

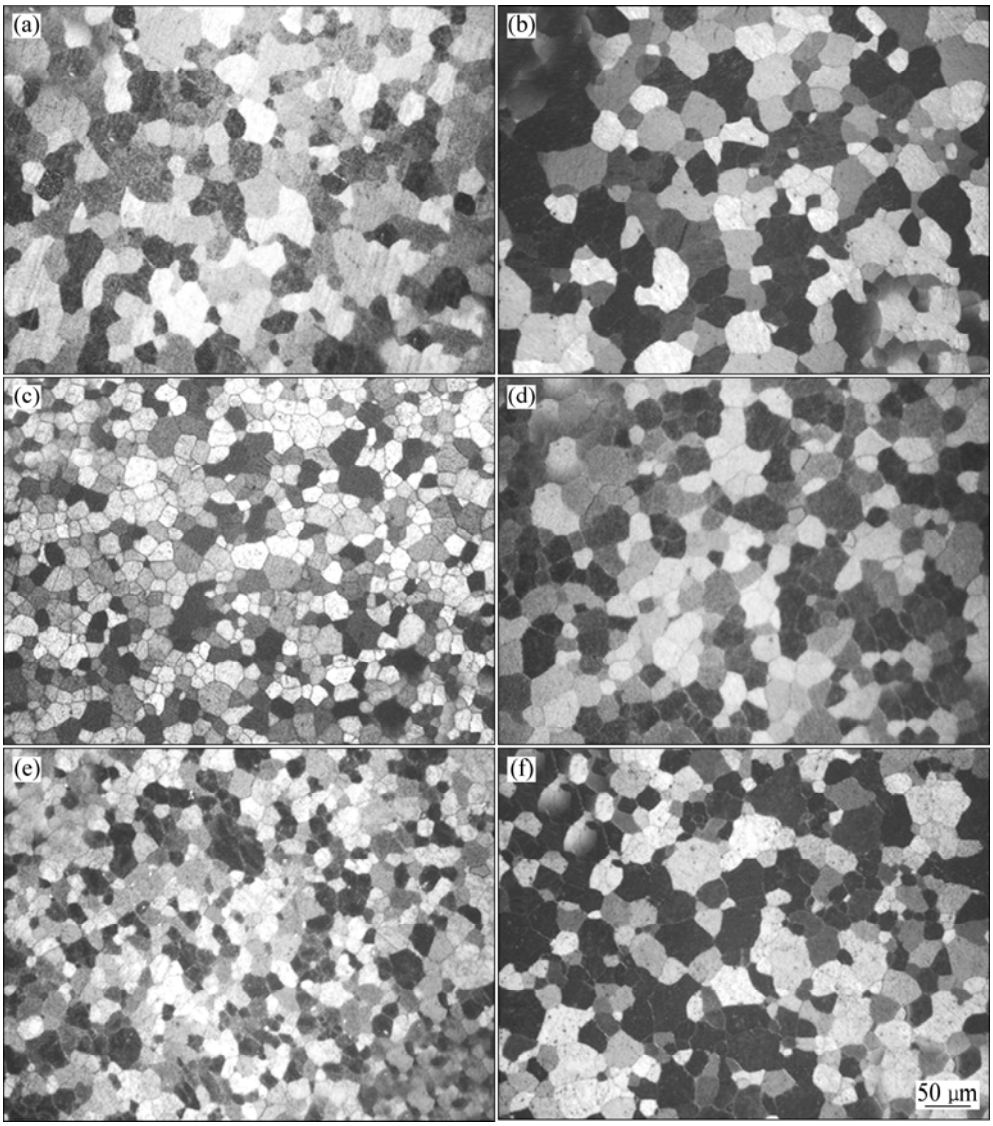

Fig.8 OM images of cross sections in two-step-aged Mg-*x*%Zn-1%Mn alloys with different *x* values: (a) *x*=4; (b) *x*=5; (c) *x*=6; (d) *x*=7; (e) *x*=8; (f) *x*=9

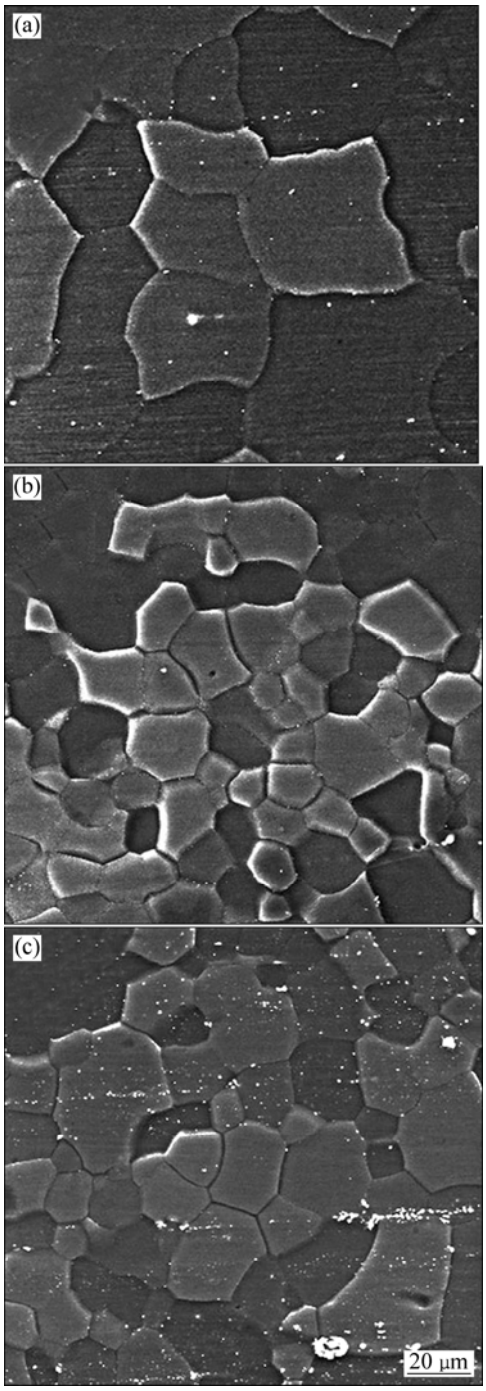

Fig.9 SEM images of T6 treated Mg-*x*%Zn-1%Mn alloy with different *x* values: (a) *x*=4; (b) *x*=6; (c) *x*=9 (parallel to extrusion direction)

420 °C, resulting in supersaturated solid solution after water quenching, the microstructures are shown in Figs.9(a) and (b), few visible particles may be high-melting-point pure Mn or Mn-Zn compounds since a huge number of nanophases stemming from aging treatment cannot be observed; on the other hand, Zn contents in ZM71, ZM81 and ZM91 alloys exceed the solid solubility limit of Zn in Mg-Zn system, so residual streamlines still can be seen in these high-zinc alloys(Fig.9(c)).

$MgZn_2$ and pure Mn can be indexed in the XRD pattern of ZM91 alloy in T6 condition (Fig.10). Mg_7Zn_3 phase no longer exists after T6 treatment and the diffraction peaks of $MgZn_2$ broaden. According to Scherrer formula, peak broadening qualitatively illustrates a decrease of grain size in the corresponding phase, implying that $MgZn_2$ phases precipitated in aging process are very thin.

The SEM microstructure and EDS analysis of two-step-aged ZM91 alloy are shown in Fig.11 and Table 6, respectively. It can be observed that three types of precipitates are present. One is a tiny rod-shaped phase (marked as *A*), the Mn content of this small region *A* is

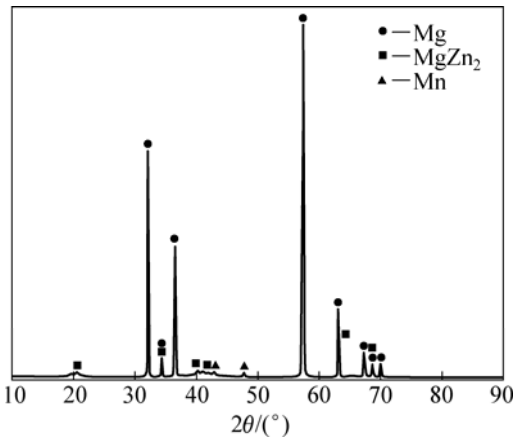

Fig.10 XRD pattern of Mg-9Zn-1Mn alloy in T6 condition

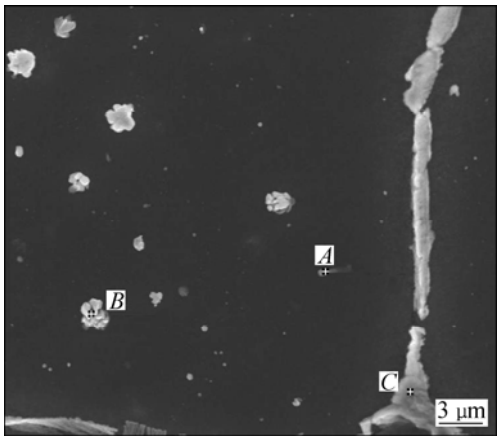

Fig.11 SEM image of two-step aged ZM91 alloy

Table 6 EDS analysis result of two-step aged ZM91 alloy in Fig.11 (mass fraction, %)

Position	O	Mg	Mn	Zn	Total
A	2.31	55.46	33.66	8.58	100.00
B	3.83	65.62	3.07	27.48	100.00
C	16.05	52.49	0.62	30.83	100.00

up to 33% (mass fraction), which can be identified as a pure Mn phase in the view of the fact that the sphere acted by electronic beam in point analysis covers quite a part of α-Mg matrix. The other is a spherical phase (marked as *B*) enriched with Zn (27%), which should be a Mg-Zn compound, meanwhile, some Mn atoms(3%) gather at the region *B*; the spherical phases disperse within the grain and generally take up a large volume, therefore, they may be incoherent with the matrix, and their strengthening effect is limited. The third is a continuous network phase along the grain boundary (marked as *C*) which is definitely a Mg-Zn compound since it consists of 30% Zn and merely 0.62% Mn; these network phases will gravely damage the ductility and cause brittle failure. Moreover, in an alloy with Zn such as ZM91, local melting may take place at grain boundaries during the solution treatment, and then coarse eutectic Mg-Zn compounds (marked as *C*) form during the water quenching. On the other hand, spherical Mg-Zn compounds (marked as *B*) may be also eutectic colonies since larger residual streamlines are also easy to melt at 420 °C. However, huge amount of nano-sized Mg-Zn particles precipitated during aging process cannot be seen in this SEM image.

3.4 Effect of Zn content on mechanical properties

Table 7 lists the tensile properties of Mg-*x*%Zn-1%Mn alloys in as extruded, T6 and T4+two-step-aging conditions, the relationship between tensile properties and Zn content is shown in Fig.12.

Variations in yield strength as a function of Zn content is shown in Fig.12(a). ZM41 alloy possesses almost the same yield strength no matter which condition it is in, besides, aged alloys exhibit much higher yield strength than extruded ones; on the other hand, two-step-aged alloys exhibit higher yield strength than one-step-aged ones. The yield strength of extruded alloys tends to go down slightly with the increase of Zn content, yet ZM61 alloy possesses particularly low yield strength. According to Hall-Petch law, the relationship between the yield strength and the gain size can be described as $\sigma_s=\sigma_0+kd^{-1/2}$, where σ_0 and k are constants, d is the grain size, the value of k reflects the sensitivity of the yield strength to the grain size. Magnesium has a relatively high k value of 0.3−0.47[16], so extruded ZM61 alloy (Fig.5) with the largest average grain size possesses the lowest yield strength, and ZM41 alloy with the smallest grains possesses the highest yield strength. The yield strength of alloys in both one-step-aged and two-step-aged condition shows a parabola-growth with the increase of Zn content, that is the yield strength undertakes a linear increase as Zn content rises from 4% to 6%, and then there is only a slight increase even if more Zn is added.

Fig.12(a) also shows the relationship between the ultimate tensile strength and Zn content. The tensile

Table 7 Tensile properties of Mg-*x*%Zn-1%Mn alloys in extruded, T6 treated and T4+two-step aged conditions

Alloy	Condition	Yield strength/MPa	Ultimate tensile strength/MPa	Elongation/%
ZM41	As-extruded	239	299	11.63
	T6	235	278	7
	T4+two-step-aging	243	284	6.04
ZM51	As-extruded	235	312	13.33
	T6	262	304	6.93
	T4+two-step-aging	293	325	4.79
ZM61	As-extruded	209	305	11.55
	T6	314	352	7.98
	T4+two-step-aging	338	366	5.2
ZM71	As-extruded	222	311	13.1
	T6	334	363	3.47
	T4+two-step-aging	343	370	4.34
ZM81	As-extruded	227	320	13
	T6	331	349	0.44
	T4+two-step-aging	356	382	1.86
ZM91	As-extruded	225	327	14.4
	T6	343	374	2.55
	T4+two-step-aging	355	378	1.67

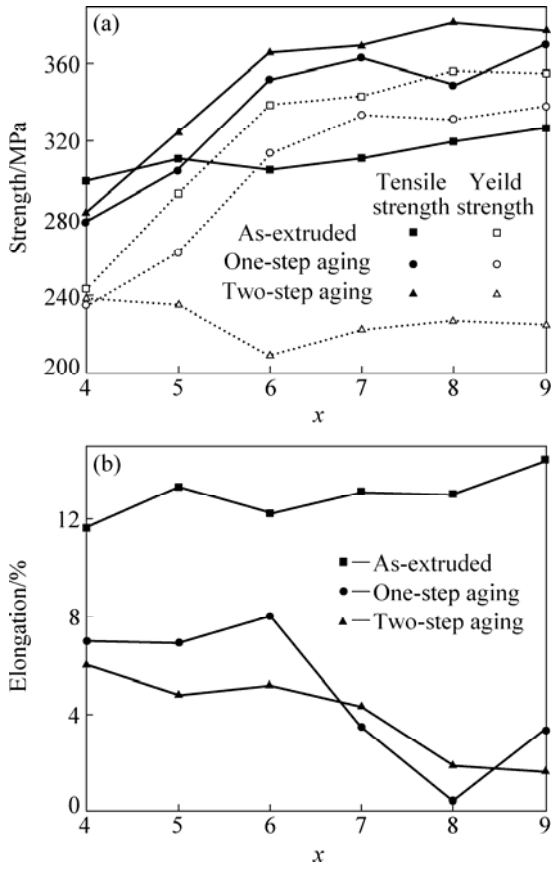

Fig.12 Effect of Zn content on mechanical properties of Mg-*x*%Zn-1%Mn wrought Mg alloys: (a) Yield strength and ultimate tensile strength; (b) Elongation

strength of extruded alloys is not very sensitive to Zn content. As mentioned above, the DRC grains during hot extrusion have a tendency to grow up as Zn content increases, which weakens the strengthening effect obtained from grain refinement; on the other hand, the dispersoids in extruded alloys are much coarser and incoherent with the matrix, so their strengthening effect is limited; these two aspects explain the insensitivity of tensile strength with increasing Zn content. Aging treatment can largely increase the tensile strength; however, the basic principle is not suitable for alloys with lower Zn content, like ZM41 and ZM51. High strength after aging treatment is mainly due to the presence of a huge amount of fine and homogeneously distributed Mg-Zn dispersoid particles. By contrast, strengthening phases in ZM41 and ZM51 are not enough and their resultant grain size are much larger, resulting in the phenomenon that the tensile strength of aged alloys is inferior to that of extruded ones. As the case with the yield strength of aged alloys, a parabola-growth also can be seen in the tensile strength of aged alloys and the turning point occurs at 6% of Zn content. As mentioned previously, 6.2% is the maximum solid solubility of Zn in Mg-Zn system, over-added Zn cannot dissolve into matrix to form supersaturated solid solution, then it is impossible for the additional Zn to form coherent nano-sized $MgZn_2$ dispersoid particles during aging treatment, therefore, even a Zn content higher than 6% cannot bring a sharp rising to the strength. Furthermore, two-step aging shows a better strengthening effect than one-step aging. Because the temperature of pre-aging is lower, the supersaturation of Zn is much higher as compared with the higher aging temperature, thus the driving force for nucleation is larger, which in turn leads to a higher density of GP zones and a higher density of $MgZn_2$ precipitates in the second stage of aging, providing better dispersion strengthening than one-step aging.

The relationship between the elongation and Zn content is represented in Fig.12(b). The elongation of extruded alloys steadily maintains a relatively high level (around 12%) no matter how much Zn is added, suggesting that larger particles in streamlines have a very tough bond with the matrix and their movements can be beautifully coordinated. Thus, even more streamlines in the microstructure cannot decrease the elongation. On the other hand, alloys after aging treatment show a much lower elongation than extruded alloys, indicating that nano-sized dispersoid particles which are coherent with the matrix can more effectively hinder the motion of dislocations than larger particles in extruded alloys. Moreover, for aged alloys, while Zn content exceeds 6%, a network of Mg-Zn precipitates appears along grain boundaries, which can sharply aggravate the elongation.

A detailed analysis makes it clear that ZM61 alloy after extrusion and aging treatment has the best combination property, since it gets a higher strength and meanwhile the elongation is not severely lowered.

4 Conclusions

1) Recrystallized grains tend to grow up as Zn content increases; meanwhile, more streamlines form. Adding more Zn will bring strong inhibition to grain growth during the solution treatment at 420 °C, resulting in finer resultant grains.

2) Coherent nano-sized $MgZn_2$ precipitates in aged alloys bring effective hardening effect. Huge amount of GP zones formed during the pre-aging act as effective nucleation sits for $MgZn_2$ phases in following aging, leading to much better strengthening effect.

3) Tensile properties of extruded alloys are not very sensitive to the variation of Zn content. As Zn content increases from 4% to 6%, both the yield and tensile strengths of aged alloys rise linearly, but the increase rate largely slows down while Zn content is more than 6%, the extra Zn over 6% can severely deteriorate the elongation. Consequently, 6% is the best Zn content for

the Mg-*x*%Zn-1%Mn alloys to possess the optimum combination property.

References

[1] OH-ISHI K, HONO K, SHIN K S. Effect of pre-aging and Al addition on age-hardening and microstructure in Mg-6 wt% Zn alloys [J]. Materials Science and Engineering A, 2008, 496(1−2): 425−433.

[2] WEI Liu-ying, DUNLOP G L, WESTENGEN H. Precipitation hardening of Mg-Zn and Mg-Zn-RE alloys [J]. Metallurgical and Materials Transactions A, 1995, 26(7): 1705−1716.

[3] CHUN J S, BYRNE J G. Precipitate strengthening mechanisms in magnesium zinc alloy single crystals [J]. Journal of Materials Science, 1969, 4(10): 861−872.

[4] GAO Xiang, NIE Jian-feng. Characterization of strengthening precipitate phases in a Mg-Zn alloy [J]. Scripta Materialia, 2007, 56(8): 645−648.

[5] GAO Xiang, NIE Jian-feng. Structure and thermal stability of primary intermetallic particles in an Mg-Zn casting alloy [J]. Scripta Materialia, 2007, 57(7): 655−658.

[6] PARK S S, BAE G T, KANG D H, JUNG I H, SHIN K S, KIM N J. Microstructure and tensile properties of twin-roll cast Mg-Zn- Mn-Al alloys[J]. Scripta Materialia, 2007, 57(9): 793−796.

[7] PARK S S, OH Y S, KANG D H, KIM N J. Microstructural evolution in twin-roll strip cast Mg-Zn-Mn-Al alloy [J]. Materials Science and Engineering A, 2007, 449−451: 352−355.

[8] LI Wen-xian. Magnesium and its alloys [M]. Changsha: Central South University Press, 2005: 349−352. (in Chinese)

[9] BUHA J. Characterisation of precipitates in an aged Mg-Zn-Ti alloy [J]. Journal of Alloys and Compounds, 2009, 472(1−2): 171−177.

[10] BUHA J. The effect of micro-alloying addition of Cr on age hardening of an Mg-Zn alloy[J]. Materials Science and Engineering A, 2008, 492(1−2): 293−299.

[11] PING D H, HONO K, NIE Jian-feng. Atom probe characterization of plate-like precipitates in a Mg-RE-Zn-Zr casting alloy [J]. Scripta Materialia, 2003, 48(8): 1017−1022.

[12] OH J C, OHKUBO T, MUKAI T, HONO K. TEM and 3DAP characterization of an age-hardened Mg-Ca-Zn alloy [J]. Scripta Materialia, 2005, 53(6): 675−679.

[13] SHAHZAD M, WAGNER L. Microstructure development during extrusion in a wrought Mg-Zn-Zr alloy [J]. Scripta Materialia, 2009, 60(7): 536−538.

[14] KIM J H, KIM J H, YEOM J T, LEE D G, LIM S G, PARD N K. Effect of scandium content on the hot extrusion of Al-Zn-Mg-(Sc) alloy [J]. Journal of Materials Processing Technology, 2007, 187−188: 635−639.

[15] DAI Qing-wei, ZHANG Ding-fei, YUAN Wei. Researches on extrusion, microstructure and mechanical properties of the new Mg-Zn-Mn alloy [J]. Materials Engineering, 2008, 299(4): 38−42. (in Chinese)

[16] ZHANG Er-lin, YIN Dong-song, XU Li-ping, YANG Lei, YANG Ke. Microstructure, mechanical and corrosion properties and biocompatibility of Mg-Zn-Mn alloys for biomedical application [J]. Materials Science and Engineering C, 2009, 29(3): 987−993.

Mg-*x*%Zn-1%Mn(*x*=4, 5, 6, 7, 8, 9)变形镁合金的组织演变和力学性能

张丁非[1,2]，石国梁[1]，赵霞兵[1]，齐福刚[1]

1. 重庆大学 材料科学与工程学院，重庆 400045；2.国家镁合金材料工程技术研究中心，重庆 400044

摘　要：研究不同 Zn 含量的 Mg-*x*%Zn-1%Mn(*x*=4, 5, 6, 7, 8, 9) 变形镁合金经热机械处理后的显微组织和力学性能的演变。在热挤压过程中，显微组织经动态再结晶得以充分细化。随着 Zn 含量的增加，动态再结晶晶粒有长大的趋势，然而，随之增加的第二相流线阻碍其长大。固溶处理使动态再结晶晶粒快速长大，但高 Zn 含量会阻碍晶界迁移，从而使最终的晶粒较为细小。在单级时效过程中，与基体共格的 $MgZn_2$ 弥散相会从过饱和固溶体中析出；在双级时效时，预时效过程中析出的大量纳米尺度的 GP 区为第二级时效过程中 $MgZn_2$ 相的析出提供了有效的异质形核核心，从而使该强化相的弥散度增加。挤压态试样的力学性能对 Zn 含量的变化不敏感，抗拉强度在 300−320 MPa 之间波动，伸长率在 11%−14%之间波动。时效态试样的强度随着 Zn 含量的增加以抛物线形式增加，单级时效态试样的抗拉强度从 278 MPa 增加到 374 MPa，而双级时效态试样的抗拉强度从 284 MPa 增加到 378 MPa，但所有试样的伸长率都小于 8%。当 Zn 含量超过其在 Mg-Zn 二元合金体系中的最大固溶度(约 6.2%)后，合金的强度增加缓慢但伸长率却迅速降低。因此，含 6%Zn 的 Mg-Zn-Mn 合金具有最佳的力学性能，即经过单级和双级时效后，合金的抗拉强度分别为 352 MPa 和 366 MPa, 伸长率分别为 8%和 5%。

关键词：Mg-Zn-Mn 合金；双级时效；时效硬化；Zn 含量

(Edited by FANG Jing-hua)